# Cyclotron Motion in the Vicinity of a Lifshitz Transition in Graphite

M. Orlita,[1,2] P. Neugebauer,[1] C. Faugeras,[1] A.-L. Barra,[1] M. Potemski,[1] F. M. D. Pellegrino,[3,4] and D. M. Basko[5]

[1]*Laboratoire National des Champs Magnétiques Intenses, CNRS-UJF-UPS-INSA, Grenoble, France*
[2]*Charles University, Faculty of Mathematics and Physics, Ke Karlovu 5, 121 16 Praha 2, Czech Republic*
[3]*Dipartimento di Fisica e Astronomia, Università di Catania, Via S. Sofia 64, I-95123 Catania, Italy*
[4]*CNISM, UdR Catania, I-95123 Catania, Italy*
[5]*Université Grenoble 1/CNRS, LPMMC UMR 5493, B.P. 166, 38042 Grenoble, France*

(Received 21 September 2011; published 4 January 2012)

Graphite, a model (semi)metal with trigonally warped bands, is investigated with a magnetoabsorption experiment and viewed as an electronic system in the vicinity of the Lifshitz transition. A characteristic pattern of up to 20 cyclotron resonance harmonics has been observed. This large number of resonances, their relative strengths and characteristic shapes trace the universal properties of the electronic states near a separatrix in momentum space. Quantum-mechanical perturbative methods with respect to the trigonal warping term hardly describe the data which are, on the other hand, fairly well reproduced within a quasiclassical approach and conventional band structure model. Trigonal symmetry is preserved in graphite in contrast to a similar system, bilayer graphene.

DOI: 10.1103/PhysRevLett.108.017602 PACS numbers: 76.40.+b, 71.70.Di, 73.22.Pr, 81.05.uf

A Lifshitz transition [1] (also known as electronic topological transition) is a change in the Fermi surface topology occurring upon a continuous change of some external parameter, such as pressure [2], magnetic field [3] or, most naturally, doping [4]. This transition does not involve symmetry breaking, like conventional phase transitions of the Landau type, but still leads to observable singularities in thermodynamics, electron transport, sound propagation, and magnetic response of metals [5]. Saddle points in electronic dispersion, often apparent in complex metals, have only recently been visualized with the spectroscopy method of angle-resolved photoemission [6]. In this Letter, we show how the proximity to a Lifshitz transition manifests itself in cyclotron resonance (CR) absorption experiments on graphite, a model system with saddle points due to the trigonal warping of electronic bands [7].

Classically, CR can be understood from the equation of motion for an electron in a magnetic field $\mathbf{B}$ [8]:

$$d\mathbf{p}/dt = (e/c)[\mathbf{v} \times \mathbf{B}], \tag{1}$$

where $\mathbf{p} = \hbar\mathbf{k}$ is the electron quasimomentum, $e = -|e|$ the electron charge, and $\mathbf{v} = \partial\epsilon(\mathbf{p})/\partial\mathbf{p}$ is the electron velocity, determined by the dispersion $\epsilon(\mathbf{p})$. Since both the energy $\epsilon$ and the momentum component $p_z$ along $\mathbf{B}$ are conserved, the motion occurs along cyclotron orbits in the $(p_x, p_y)$ plane, determined by the condition $\epsilon(p_x, p_y, p_z) = \text{const}$. This motion is periodic, and its period, $2\pi/\omega_c$, being proportional to the cyclotron mass, defines the cyclotron frequency $\omega_c = \omega_c(\epsilon, p_z)$. When an electric field, oscillating at frequency $\omega$, is applied, the electron can absorb energy. Absorption becomes resonant when the perturbation frequency $\omega$ matches the cyclotron frequency $\omega_c$ or its integer multiple.

In good metals, the incoming radiation is efficiently screened and penetrates the sample only within a thin skin layer. CR absorption is then a surface effect, observed mainly when the magnetic field is parallel to the surface [9,10]. This makes CR for good metals a less efficient tool for probing the Fermi surface, as compared to other methods, such as, e.g., the de Haas–van Alphen effect. The resonant absorption is also often smeared by the dependence of $\omega_c$ on $p_z$, which is an additional disadvantage.

We have applied the CR absorption technique to study the cyclotron motion in the vicinity of the Lifshitz transition in graphite. The low-temperature in-plane conductivity of this material is relatively low, $\sigma \sim 10^7$–$10^8$ $(\Omega \cdot \text{m})^{-1}$, and it quickly decreases upon the application of a magnetic field [7,11]. The skin depth thus reaches tens of nanometers and greatly exceeds the spacing between adjacent graphene layers. Moreover, graphite is a highly anisotropic crystal with rather flat electronic dispersion in the $z$ direction (perpendicular to the layers). It appears as a suitable material for CR studies of the electronic system near the Lifshitz transition driven by the trigonal warping of electronic bands.

CR absorption was measured using the setup routinely applied to high-frequency electron paramagnetic resonance experiments [12]. A flake of natural graphite (50 $\mu$m thick, area 1 mm$^2$) was placed in a Fabry-Perot cavity mounted inside a superconducting coil. The magnetic field was applied perpendicular to the graphene layers. Linearly polarized microwave radiation from a Gunn diode tripled to a frequency of 283.2 GHz (1.171 meV) was delivered to the sample via quasioptics waveguides. The field-modulation technique was applied to enhance the detection sensitivity. The modulation

 

amplitude was chosen in a way to maximize the signal but to not distort the measured line shapes.

A representative experimental spectrum (raw data) is shown in Fig. 1(a). This trace represents the response of the natural graphite specimen measured as a function of the magnetic field at fixed microwave frequency. Because of the field-modulation technique, it corresponds to the derivative of the absorbed power with respect to $B$. The magnetoabsorption response of graphite is expected to be mostly sensitive to singularities in the electronic joint density of states, located at the $K$ and $H$ points of the graphite Brillouin zone. A number of the observed resonances can be easily identified as being due to electronic states at the $K$ point, along the results of previous similar studies [13–18]. Holes at the $H$ point as well as decoupled sheets of graphene on the surface of graphite give rise to resonances at a different spectral range (much lower magnetic fields) [19,20].

To a very first approximation, the $K$ point electrons of graphite have parabolic dispersion. Their effective mass, most frequently reported to be in the range from $m = 0.057m_0$ to $0.060m_0$ [7] ($m_0$ free electron mass), fixes the cyclotron frequency at $\hbar\omega_{c0} \approx 2 \times B[\mathrm{T}]$ meV. Then, the broad but still visible resonance at $|B| \approx 0.6$ T is attributed to the fundamental CR absorption. All other observed resonances are higher harmonics of the fundamental one. This is evidenced in Fig. 1(b) where the spectrum from Fig. 1(a) is replotted against $\omega/\omega_{c0}$ (i.e., versus $B^{-1}$ instead of $B$). $\hbar\omega_{c0}$ is eventually set at $2.05 \times B[\mathrm{T}]$ meV. In agreement with previous reports [13], the observed harmonics follow two series: $\omega \approx |3k \pm 1|\omega_{c0}$, where $k = 0, \pm 1, \pm 2 \ldots$.

The superior quality of the present data (due to higher frequencies applied and perhaps a better quality of graphite specimens) allows us to uncover more and intriguing spectral features. Our key observations, that we interpret in the following, are (i) the appearance of a large number (up to 20) of CR harmonics, (ii) an enhanced strength of $3k + 1$ harmonics as compared to the strength of the $3k - 1$ series at $B > 0$ (and vice versa at $B < 0$), and finally, (iii) a very characteristic, asymmetric broadening of the observed resonances, enhanced on the low-frequency (high-field) sides of the absorption peaks. These features are clearly seen in the raw data and also in Fig. 1(c) in which we reproduce the actual absorption spectrum, as derived from the numerical integration, over the magnetic field, of the measured (differential) signal.

The appearance of $n$ harmonics with $n = 3k \pm 1$ is usually understood as being due to breaking of the isotropy of the electronic spectrum in the layer plane by the trigonal warping. For isotropic bands, only the $k = 0$ fundamental transition is allowed, whereas the $n = 3k \pm 1$ harmonic appears in the $|k|$th order of the perturbation theory with respect to the trigonal warping term [16,21]. The spectrum in Fig. 1 contains many harmonics which start to fall off only at large indices $n \gtrsim 7$. Clearly, the perturbation theory is not applicable to interpret these data. Instead, we will use the quasiclassical approximation.

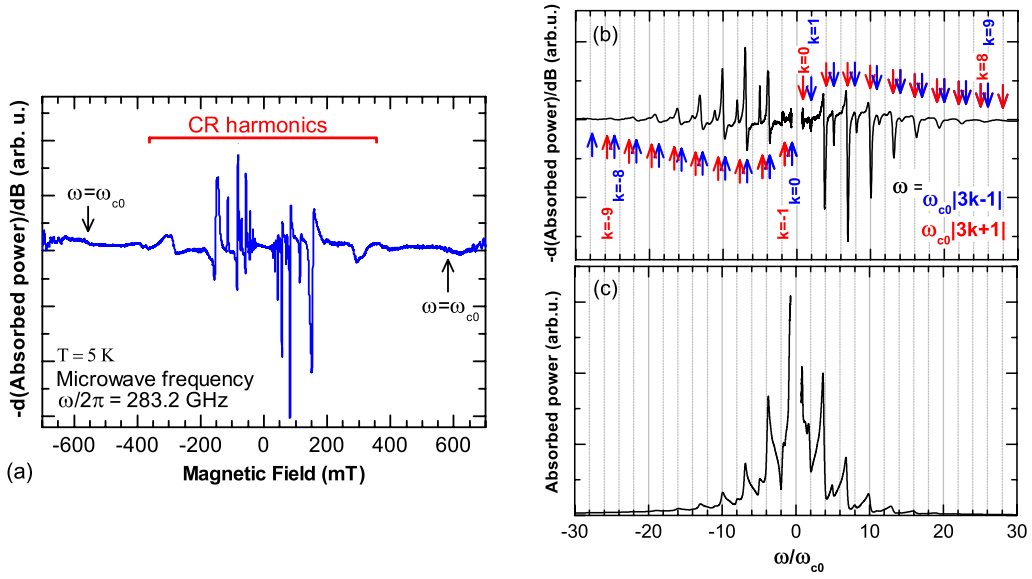


FIG. 1 (color online). Magnetoabsorption spectra of natural graphite measured at a fixed microwave excitation energy $\hbar\omega = 1.171$ meV and detected with the help of the field-modulation technique at temperature of 5 K. Harmonics of fundamental CR frequency $\omega_{c0} = eB/m_{c0}$ ($m_{c0} = 0.057m_0$) are observed down to fields of 20 mT. (a) Derivative of the absorption with respect to the magnetic field $B$, as a function of $B$. (b) The same plotted as a function of $\omega/\omega_{c0}$, so that individual harmonics at frequencies of $|3k \pm 1|\omega_{c0}$, $k = 0, \pm 1, \pm 2 \ldots$, are clearly seen, as marked by vertical arrows. (c) Absorption as a function of $\omega/\omega_{c0}$ obtained by the numerical integration of the curve presented in part (a) with respect to $B$.

Equation (1) can be cast in the Hamiltonian form in the phase space $(p_x, p_y)$: $dp_x/dt = -\partial\mathcal{H}(p_x, p_y)/\partial p_y$, $dp_y/dt = \partial\mathcal{H}(p_x, p_y)/\partial p_x$, with the Hamiltonian $\mathcal{H}(p_x, p_y) = -(eB/c)\epsilon(p_x, p_y)$ (we omitted $p_z$, which enters as a parameter). Generally, classical Hamiltonian systems exhibit a very rich behavior. However, they share some universal features when the energy $\epsilon$ is close to that of a saddle point of the Hamiltonian, $\epsilon = \epsilon_{\rm sp}$, as is well known in the classical nonlinear physics [22]. (i) The cyclotron motion in the vicinity of a saddle point is slow and its period diverges logarithmically, $\omega_c(\epsilon) \to 0$ for $\epsilon \to \epsilon_{\rm sp}$. (ii) The Fourier spectrum of this motion contains many harmonics and their number diverges when $\epsilon \to \epsilon_{\rm sp}$. This second fact provides an obvious hint for the interpretation of the experimental data.

The experimentally probed electronic states are those around the Fermi level $\epsilon_F$. Thus, the effects discussed above are important if $\epsilon_F \approx \epsilon_{\rm sp}$. This is the case of graphite, as illustrated in Fig. 2 using standard calculations based on the Slonczewski-Weiss-McClure (SWM) model [23] in the two-band approximation (see Supplemental Information [24]). Here we used the standard values of the SWM parameters [7]: $\gamma_0 = 3150$ meV, $\gamma_1 = 375$ meV, $\gamma_2 = -20$ meV, $\gamma_3 = 315$ meV, $\gamma_4 = 44$ meV, $\gamma_5 = 38$ meV, $\Delta = -8$ meV. The band dispersion has six saddle points at two different energies $\epsilon_{e\text{-sp}}$ and $\epsilon_{h\text{-sp}}$, which define two separatrices—isoenergetic lines separating regions with different topology. Fermi level crossing these saddle points would imply the change in the topology of the Fermi surface, which actually corresponds to the Lifshitz transition of the neck-collapsing type. The Fermi level is close to the upper separatrix, on which we focus our attention hereafter, $\epsilon_{\rm sp} \equiv \epsilon_{e\text{-sp}}$. The single electron pocket around the $K$ point at $\epsilon_F > \epsilon_{\rm sp}$, splits into four disconnected pockets when $\epsilon_F$ goes below $\epsilon_{\rm sp}$. Figure 2(d) shows the classical cyclotron frequency for the SWM dispersion at $k_z = 0$, which vanishes at $\epsilon = \epsilon_{\rm sp}$.

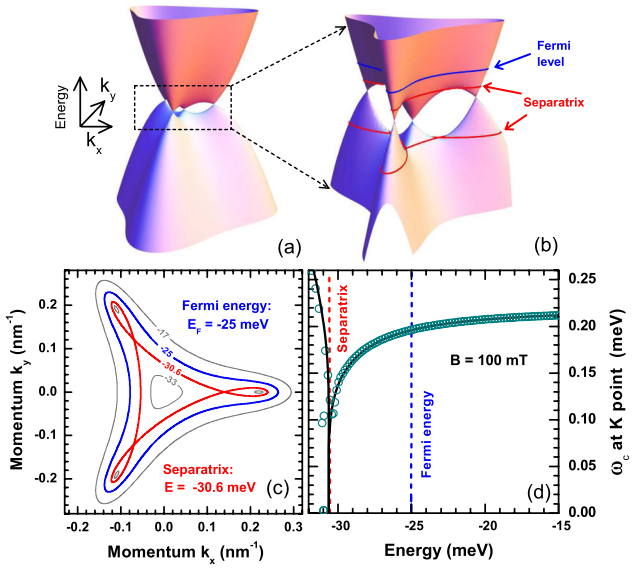


FIG. 2 (color online). (a),(b) Electronic structure near the $K$ point of graphite ($k_z = 0$). Two separatrix lines pass through six saddle points. The Fermi level is located about 6 meV above the upper separatrix. (c) Constant energy contours in the $(k_x, k_y)$ plane for $k_z = 0$ for $\epsilon = -17$, $\epsilon = -25$ (Fermi level), $\epsilon = -30.6$ (upper separatrix), and $\epsilon = -33$ meV. (d) Classical cyclotron frequency $\hbar\omega_c(\epsilon, k_z = 0)$ at $B = 100$ mT in the relevant energy interval. $\omega_c$ vanishes at the saddle point. Open circles show the LL spacing, $\Delta\epsilon_l = \epsilon_{l+1} - \epsilon_l$, as a function of $\epsilon_l$, derived from the SWM model. Roughly 1 meV away from the saddle point, the circles fall on the classical curve, $\Delta\epsilon_l \approx \hbar\omega_c(\epsilon_l)$.

In the language of quantum mechanics, the $k_z = 0$ energy spectrum consists of discrete Landau levels (LLs) $\epsilon_l$. In the quasiclassical approximation, $\epsilon_l$ can be found from the Bohr-Sommerfeld quantization rule. The $n$th CR harmonic corresponds to the transition over $n$ levels, $n\hbar\omega_c \approx \epsilon_{l+n} - \epsilon_l$, to the leading order in $\hbar$. The decrease of $\omega_c(\epsilon)$ at $\epsilon \to \epsilon_{\rm sp}$ corresponds to an accumulation of LLs. Nevertheless, $\Delta\epsilon$ does not approach zero, since the condition of the validity of the quasiclassical quantization, $|\omega_c(\epsilon + \hbar\omega_c) - \omega_c(\epsilon)| \ll \omega_c(\epsilon)$, holds only if $\epsilon$ is not too close to $\epsilon_{\rm sp}$. LLs always remain discrete, see Fig. 2(d).

As we will show later, $\epsilon_F - \epsilon_{\rm sp}$ is about 6 meV; i.e., it is 5 times larger than the microwave frequency, $\hbar\omega = 1.171$ meV. Our classical approximation is justified in this case. As a matter of fact, the quasiclassical approximation works better, the smaller $\omega$ is. However, if microwave frequency is too small, the harmonic structure will be smeared by broadening of electronic states. The optimal frequency, used in the experiment, is thus determined by an appropriate compromise between these two competing conditions.

Assuming that the absorbed power is proportional to the real part of the conductivity, $\mathrm{Re}\sigma_{xx}(\omega)$, and calculating the latter from the standard kinetic equation [8] in the simplest relaxation time approximation for the collision integral (see Supplemental Information [24]), we obtain

$$\mathrm{Re}\,\sigma_{xx}(\omega) = \frac{e^2}{\pi^2\hbar}\sum_{n=-\infty}^{\infty}\int\left(-\frac{\partial f}{\partial\epsilon}\right)\frac{\Gamma m_c|v_{x,n}|^2 dk_z d\epsilon}{\hbar^2(\omega - n\omega_c)^2 + \Gamma^2}, \tag{2}$$

where the $k_z$ integration is from $-\pi/(2a_z)$ to $\pi/(2a_z)$. Both the cyclotron frequency, $\omega_c$, and the cyclotron mass, $m_c = -eB/(c\omega_c)$, depend on $\epsilon$ and $k_z$. The basic frequency $\omega_{c0}$, introduced earlier, is $\omega_{c0} = \omega_c(\epsilon = \epsilon_F, k_z = 0)$. $\mathbf{v}_n = \mathbf{v}_n(\epsilon, k_z)$ is the Fourier harmonic of the electron velocity, corresponding to the term $\propto e^{-in\omega_c t}$, determined from the solution of the unperturbed equation of motion, Eq. (1). Finally, $\Gamma$ accounts for relaxation, and $f(\epsilon)$ is the Fermi function.

Even without solving Eq. (1), it is easy to see that the triangular symmetry of $\epsilon(\mathbf{p})$ in the $(p_x, p_y)$ plane fixes $\mathbf{v}_n = 0$ for $n = 3k$, $k = \pm 1, \pm 2, \ldots$. In Fig. 1(b), the resonances at $n = 3k$ are absent, which demonstrates that the triangular symmetry is not broken in graphite. This is in contrast with recent reports for a bilayer graphene [25–28], even though it is formally described by the same single-particle Hamiltonian (for a fixed $k_z$) [29]. The same symmetry fixes $v_{n,x}$ to be real and $v_{n,y} = \pm i v_{n,x}$ for $n = 3k \pm 1$, so the peaks at $n = 3k + 1$ and $n = 3k - 1$ are seen in the opposite circular polarizations of the microwave field. This helps us to understand the observed difference in the intensities of the $n = 3k + 1$ and $n = 3k - 1$ series. Indeed, for $B > 0$, when the electron moves along the Fermi surface, shown in Fig. 2(b), in the overall counterclockwise direction, it should be more strongly coupled to the counterclockwise polarized radiation. As both circular polarizations are equally present in the incoming linearly polarized radiation, the spectrum is fairly symmetric with respect to $B \to -B$.

The present studies are restricted to bulk graphite, a system with fixed Fermi level but in an apparent proximity to the Lifshitz transition. An obvious experimental challenge would be to trace the CR response when changing the Fermi level with respect to the separatrix energy, with an attempt to tune the proximity to Lifshitz transition in graphitic structures. This can be in principle envisaged for electrostatically gated bilayer graphene [27,28] and/or for bulk graphite under hydrostatic pressure [30]. Importantly, such experiments require no degradation of the quality of the sample, which likely excludes the experiments on, for example, chemically doped structures.

Besides the large number of harmonics, typical of a classical motion near a saddle point, the proximity to the Lifshitz transition also leads to some lowering of the cyclotron frequency. Indeed, the fundamental cyclotron frequency determined from the period in $B^{-1}$ of the spectrum, $\hbar\omega_{c0}/B = 2.05$ meV/T, is slightly lower than its parabolic-band limit at $k_z = 0$, 2.24 meV/T. The latter value, however, relies on the specific values of the parameters of the SWM model. More apparent effects are deduced from the analysis of the peak shapes (which are determined by the integration over $k_z$).

As seen from Fig. 1(c), each peak has an abrupt cutoff on the high-frequency side and a tail on the low-frequency side. This contradicts the first intuition, based on the well-known fact that the parabolic part of the bands becomes steeper as $k_z$ increases from the $K$ point towards the $H$ point. This pushes the LLs upwards as $k_z$ increases and would result in a tail on the high-frequency side of each peak in the absorption spectrum $\mathcal{A}(\omega, B)$ [31]. However, the bottom of the conduction band [defined as $\epsilon(\mathbf{p} = 0, k_z)$] and the saddle point $\epsilon_{\mathrm{sp}}(k_z)$ shift upwards upon increasing $k_z$, as $\epsilon(\mathbf{p} = 0, k_z) = 2\gamma_2 \cos k_z a_z$, $\gamma_2 < 0$. Thus, the Fermi level approaches the saddle point as $k_z$ moves away from the $k_z = 0$ point and $\omega_c(\epsilon_F, k_z)$ decreases simultaneously, see Fig. 2(d). This provides a tail on the low-frequency side of the peaks. Thus, the suppression of $\omega_c$ near the Lifshitz transition is crucial to interpret the peak asymmetry.

The spectrum derived from Eq. (2) is shown in Fig. 3, with $\epsilon_F$ and $\Gamma$ as the only adjustable parameters—the parameters of the SWM model were fixed [7]. The best agreement is obtained for $\epsilon_F = -25$ meV. If $\epsilon_F = -24$ meV, the peaks have no asymmetry, since $\omega_c(\epsilon_F = -24\ \mathrm{meV}, k_z)$ has a significant upturn on increasing $k_z$. When $\epsilon_F = -26$ meV the falloff of large-$n$ harmonics is noticeably slower than the experimental one. In other words, the closer $\epsilon_F$ is to $\epsilon_{\mathrm{sp}}$, the more harmonics are seen in the spectrum. The frequency $\omega_c(\epsilon_F = -25\ \mathrm{meV}, k_z = 0)/B = 2.03$ meV/T agrees with the experimental value, 2.05 meV/T. The value $\epsilon_F = -25$ meV is also in good agreement with the one determined independently from the charge neutrality condition (see Supplemental Information [24]), $\epsilon_F = -24$ meV. A constant value of $\Gamma = 20\ \mu$eV was assumed for the curve in Fig. 3(a). Apparently, this does not describe well the amplitudes of peaks at $n = 1$, 2: the theoretical peaks are narrower and thus more intense than the experimental ones. Better agreement is obtained under the assumption that $\Gamma \propto \sqrt{B}$ (see Ref. [32] and Supplemental Information [24]). Notably, the curve in Fig. 3(b) with $\Gamma = 0.1\sqrt{B[\mathrm{T}]}$ meV corresponds to the zero-field relaxation rate $\hbar/\tau_{B=0} = 40\ \mu$eV. The extracted value of $\tau_{B=0}$ provides the zero-field dc conductivity $\sigma = 1.2 \times 10^8\ (\Omega \cdot \mathrm{m})^{-1}$ (see Supplemental Information [24]). This is fully consistent with typical literature data [7,11] and implies a mean electron free path of 6 $\mu$m, which is, notably, comparable or even longer than the corresponding values reported for strictly 2D graphene-based structures [27,33,34].

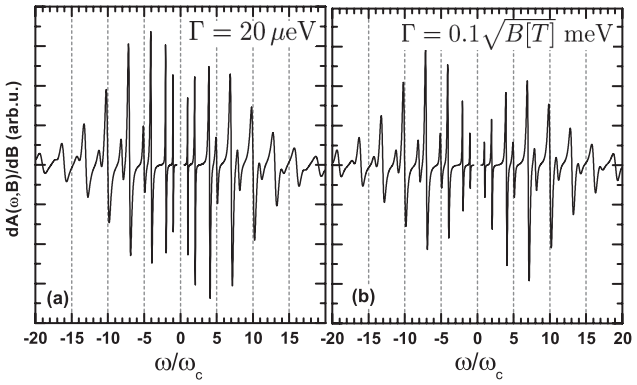


FIG. 3. Derivative of the absorption with respect to $B$, as calculated using Eq. (2) for different electronic broadenings $\Gamma$. (a) a constant broadening $\Gamma = 20\ \mu$eV and (b) $\Gamma = 0.1\sqrt{B[\mathrm{T}]}$ meV.

To conclude, we have introduced CR experiments as a new tool to study Lifshitz transitions. We have shown how the proximity to the Lifshitz transition manifests itself in the CR spectrum of a model system, bulk graphite. Namely, we have observed a multimode response, where the basic CR mode is accompanied by many harmonics. Using the standard SWM model for the electronic band structure of graphite to analyze the data, we have determined the Fermi energy and estimated the electronic broadening. The similarity between the band structure of graphite near the $K$ point and that of a bilayer graphene logically suggests to probe Lifshitz transition in the latter system by CR methods, and to shed more light on the currently debated issue of spontaneous symmetry breaking in bilayer graphene [25–28].

We thank M.-O. Goerbig and J.-N. Fuchs for collaboration on the early stages of this work, and V. F. Gantmakher and Yu. I. Latyshev for helpful discussions. Part of this work was supported by RTRA DISPOGRAPH project. M. O. acknowledges support from GACR P204/10/1020 and GRA/10/E006 (EPIGRAT). F. M. D. P. thanks LPMMC for hospitality.

[1] I. M. Lishitz, Zh. Eksp. Teor. Fiz. **38**, 1565 (1960).
[2] V. I. Makarov and Bar'yakhtar, Zh. Eksp. Teor. Fiz. **48**, 1717 (1965), and references therein; C. W. Chu, T. F. Smith, and W. E. Gardner, Phys. Rev. B **1**, 214 (1970); B. K. Godwal *et al.*, Phys. Rev. B **57**, 773 (1998).
[3] P. M. C. Rourke *et al.*, Phys. Rev. Lett. **101**, 237205 (2008); J. Wosnitza *et al.*, Physica (Amsterdam) **403B**, 1219 (2008).
[4] D. Yoshizumi *et al.*, J. Phys. Soc. Jpn. **76**, 063705 (2007); Y. Okamoto, A. Nishio, and Z. Hiroi, Phys. Rev. B **81**, 121102(R) (2010); S. E. Sebastian *et al.*, Proc. Natl. Acad. Sci. U.S.A. **107**, 6175 (2010); M. R. Norman, J. Lin, and A. J. Millis, Phys. Rev. B **81**, 180513(R) (2010); D. LeBoeuf *et al.*, Phys. Rev. B **83**, 054506 (2011).
[5] Y. M. Blanter *et al.*, Phys. Rep. **245**, 159 (1994).
[6] C. Liu *et al.*, Nature Phys. **6**, 419 (2010).
[7] N. B. Brandt, S. M. Chudinov, and Y. G. Ponomarev, *Semimetals 1: Graphite and Its Compounds* (North-Holland, Amsterdam, 1988).
[8] A. A. Abrikosov, *Fundamentals of the Theory of Metals* (North-Holland, Amsterdam, 1988).
[9] M. Ya. Azbel' and E. A. Kaner, Zh. Eksp. Teor. Fiz. **30**, 811 (1956).
[10] M. S. Khaĭkin, Zh. Eksp. Teor. Fiz. **41**, 1773 (1961) [Sov. Phys. JETP **14**, 1260 (1962)].
[11] X. Du *et al.*, Phys. Rev. Lett. **94**, 166601 (2005).
[12] P. Neugebauer and A.-L. Barra, Appl. Magn. Reson. **37**, 833 (2010).
[13] J. K. Galt, W. A. Yager, and H. W. Dail, Jr., Phys. Rev. **103**, 1586 (1956); S. J. Williamson *et al.*, Solid State Commun. **4**, 37 (1966); H. Suematsu and S. Tanuma, J. Phys. Soc. Jpn. **33**, 1619 (1972).
[14] B. Lax and H. J. Zeiger, Phys. Rev. **105**, 1466 (1957).
[15] P. Nozières, Phys. Rev. **109**, 1510 (1958).
[16] M. Inoue, J. Phys. Soc. Jpn. **17**, 808 (1962).
[17] G. Dresselhaus, Phys. Rev. B **10**, 3602 (1974).
[18] R. E. Doezema *et al.*, Phys. Rev. B **19**, 4224 (1979).
[19] M. Orlita *et al.*, Phys. Rev. Lett. **100**, 136403 (2008).
[20] P. Neugebauer *et al.*, Phys. Rev. Lett. **103**, 136403 (2009).
[21] D. S. L. Abergel and V. I. Fal'ko, Phys. Rev. B **75**, 155430 (2007); L. A. Falkovsky, Phys. Rev. B **84**, 115414 (2011).
[22] R. Z. Sagdeev, D. A. Usikov, and G. M. Zaslavsky, *Nonlinear Physics: From the Pendulum to Turbulence and Chaos* (Harwood Academic Publishers, New York, 1988).
[23] J. W. McClure, Phys. Rev. **108**, 612 (1957); J. C. Slonczewski and P. R. Weiss, *ibid.* **109**, 272 (1958).
[24] See Supplemental Material at http://link.aps.org/supplemental/10.1103/PhysRevLett.108.017602 for details of the SWM model as well as performed calculations of the optical conductivity.
[25] O. Vafek and K. Yang, Phys. Rev. B **81**, 041401 (2010).
[26] Y. Lemonik *et al.*, Phys. Rev. B **82**, 201408(R) (2010).
[27] A. S. Mayorov *et al.*, Science **333**, 860 (2011).
[28] M. Mucha-Kruczyński, I. L. Aleiner, and V. I. Fal'ko, Phys. Rev. B **84**, 041404 (2011).
[29] M. Orlita *et al.*, Phys. Rev. Lett. **102**, 166401 (2009).
[30] E. Mendez, A. Misu, and M. S. Dresselhaus, Phys. Rev. B **21**, 827 (1980).
[31] P. Kossacki, C. Faugeras, M. Kühne, M. Orlita, A. A. L. Nicolet, J. M. Schneider, D. M. Basko, Yu. I. Latyshev, and M. Potemski, Phys. Rev. B **84**, 235138 (2011).
[32] T. Ando, J. Phys. Soc. Jpn. **38**, 989 (1975).
[33] K. I. Bolotin *et al.*, Phys. Rev. Lett. **101**, 096802 (2008).
[34] S. A. Mayorov *et al.*, Nano Lett. **11**, 2396 (2011).